Biological Forum – An International Journal **15(3): 161-168(2023)**

ISSN No. (Print): 0975-1130
ISSN No. (Online): 2249-3239

Development and Characterization of Chitosan-Functionalized Biodegradable Nanoparticles for the Enhanced Hepatoprotective effects against Liver Fibrosis

Saurabh Arjariya[1]*, Ritesh Jain[2] and Neeraj Sharma[2]
[1]Faculty of Pharmacy, Madhyanchal professional University, Bhopal (Madhya Pradesh), India.
[2]Professor, Madhyanchal Professional University, Bhopal (Madhya Pradesh), India.

(Corresponding author: Saurabh Arjariya)*
(Received: 12 January 2023; Revised: 14 February 2023; Accepted: 18 February 2023; Published: 22 March 2023)
(Published by Research Trend)

ABSTRACT: The obstacles behind the usage of silymarin (SYL) against liver ailments has a limited oral bioavailability due to its weak water solubility and low membrane permeability, which restricts its therapeutic potential. Develop and test safe, biocompatible, Silymarin dehydroemtine-loaded chitosan nanoparticles (SYL-DH-CNPs) for hepatic administration in order to increase anti-fibrotic activity in rats with CCl4-induced liver fibrosis. The SYL-DH-CNPs was synthesized using the ionotropic gelation procedure, and they are assessed for particle size, shape, and zeta potential analysis. Successfully formulated SYL-DH-CNPs was subjected to in vivo evaluation to determine their therapeutic efficacy for 30 days of animal studies. The in vivo study showed that the synthesised SYL-DH-CNPs had a strong antifibrotic therapeutic efficacy against CCl_4 -induced hepatic damage in rats. The liver functions, inflammatory markers, antioxidant pathway activation, and lipid peroxidation reduction in SYL-DH-CNPs -treated rats were all significantly improved. They also had a healthy body weight, normal liver weight and liver index values, and reduced lipid peroxidation. Histopathology analysis confirmed the anti-fibrotic properties of SYL-DH-CNPs. Overall the findings suggested that SYL-DH-CNPs are the most effective carrier to target liver cells elevating the bioavailability at desired site and in the management of hepatic fibrosis.

Keywords: Silymarin, chronic liver disease, chitosan nanoparticles, SLY bioavailability

INTRODUCTION

The liver is one of the most prevalent organs in the human body. Bile secretion, detoxification, and the metabolism of fat, protein, and carbohydrates are the liver's main functions. Less is available in terms of contemporary medication for the principal site (Liver) for intensive metabolism and excretion (Noyan *et al.,* 2006; Thakur and Kapadnis 2021). Hepatic diseases are any physiochemical, biochemical, and morphological deviations from the liver's typical function. Liver disease refers to any abnormality in liver function that causes illness. The liver performs a number of crucial physical functions, and if it gets sick or is damaged, those functions may stop, which might be extremely harmful to the body. Liver disease is sometimes referred to as hepatic disease (Reddy *et al.,* 2019; Sethi *et al.,* 2021). Globally, chronic liver disease (CLD), which includes a wide range of illnesses with different or unidentified aetiologies, is the main cause of death. In the world, liver cirrhosis complications were directly responsible for 1.32 million deaths in 2017 (Laouar *et al.,* 2017). Hepatic fibrosis is described by Akçal as a dynamic pathophysiological process that is characterised by intrahepatic connective tissue dysplasia and results from sustained and chronic liver damage brought on by a variety of pathogenic factors (Jiao *et al.,* 2009), such as viral hepatitis, alcohol use, nonalcoholic fatty liver disease (NAFLD), nonalcoholic steatohepatitis (NASH), and toxic chemicals like carbon tetrachloride (CCl4). Liver fibrosis may eventually progress to cirrhosis and liver cancer, both of which are deadly in their advanced stages (Arfmann *et al.,* 2015). Extracellular matrix (ECM) proteins like collagen, fibronectin, and matricellular proteins are overproduced by activated hepatic stellate cells (HSCs) during hepatic fibrogenesis, which results in structural and functional abnormalities in the liver and is a key component of a cirrhotic liver. A significant hepatoprotective compound called silymarin (SLY) is obtained from milk thistle (*Silybum marianum* (L.) Gaertn) seeds. The biggest drawback of taking SIL orally is its limited absorption, despite its hepatoprotective effects (Choi *et al.,* 2009). The weak water solubility at stomach pH, poor permeability through the gut epithelial cells, and quick elimination of SIL may be the causes of its limited bioavailability (O'Reilly *et al.,* 2016). Many SLY formulations have been created to enhance the bioavailability of SLY in order to get around this problem. Dehydroemetine (DH), a synthetic antiprotozoal medication, is similar to emetine in structure and anti-amoebic properties (the key difference being a double bond next to the ethyl group), but it has less side effects (Jiang *et al.,* 2019). It is made by Roche for the American market. It used to be prescribed by the Centers for Disease Control as an experimental drug for metronidazole-resistant

amoebiasis, but they no longer do (Hobert, 2008). The bioavailability and therapeutic effects of SLY may be significantly enhanced by the nanotechnology technique (Liu *et al.,* 2018). In our earlier work, we effectively created SIL-loaded gold nanoparticles with high loading and entrapment capacities, and the in vivo investigation supported the increased anti-fibrotic actions (Ji *et al.,* 2015; Supriono *et al.,* 2019). Chitosan (CH) was chosen in the current investigation to overcome the gastrointestinal barriers to SLY bioavailability. The polymer chitosani, which is derived from natural sources, has a wide range of functional groups, mucoadhesive properties, the ability to enhance permeation, controlled drug release, and efflux inhibition (Mohseni *et al.,* 2019). Ch is a prospective candidate who satisfies the requirements for an efficient SIL delivery method because of all of these characteristics (Zhang *et al.,* 2019). It has been noted that chitosan nanoparticles (CNPs) have stronger immune-stimulating, anticancer, and antibacterial effects than those of Ch (Gjorgjieva *et al.,* 2020). The goal of the current investigation was to create and characterise silymarin-chitosan nanoparticles (SLY-DH-CNPs) that could deliver silymarin to target liver cells in an effective and targeted manner. In a rat model of CCl4-induced liver fibrosis, we looked into SLY-DH-CNPs' capacity to increase silymarin's oral administration and bioavailability as well as their anti-fibrotic activity in comparison to native SIL (Roulot *et al.,* 1999).

MATERIALS AND METHODS

The Regents and chemicals along with Silymarin medication powder and Dehydroemetine were acquired from Taj Pharmaceutical Industries (Hyderabad, India). Chitosan (deacetylation 75%, MW 160.16 (kDa)) and sodium tripolyphosphate (MW 367.86) were acquired from Oxford Lab Chem in Maharashtra, India (Mumbai, India). The highest analytical grade of additional substances and reagents was employed throughout the studies.

A. Synthesis of SLY-DH-CNPs

Chitosan nanoparticles (SLY-DH-CNPs) loaded with silymarin Dehydroemetine were created using the ionotropic gelation technique. In this procedure, negatively charged polyanion groups reacted with positively charged chitosan. In this experiment, LMW chitosan was dissolved in 100 mL of a 2% acetic acid aqueous solution to create a 2 mg/mL chitosan solution (i.e., 200 mg of chitosan was dissolved in 100 mL of acetic acid) [16]. Using a 1.0 M NaOH solution, the pH of this chitosan solution was brought down to 5. The mixture was stirred for around 40 minutes. Silymarin (SLY) and Dehydroemetine (DH) (10 mg) were dissolved in 1 mL of ethanol and sonicated for 2 minutes to create the drug solution. This solution was then added dropwise slowly into the chitosan solution, followed by the addition of 20 mL of TPP solution. Using 0.1 M HCL and steady stirring for three hours at a speed of 500 rpm with a magnetic stirrer, the pH of this solution was brought down to 5. Centrifugation of the nanoparticle suspension took place for 30 minutes at 15,000 rpm and 10 °C. The pellets were cleaned twice, redistributed in a constant amount of 10 mL of Milli-Q® water (Medical Nanotechnology Laboratory), sonicated for 20 min., and the supernatant was collected for measurement of free SLY-DH. This suspension was subsequently diluted by ten times in three millilitres, sonicated for ten minutes, and examined for characteristics including particle size, size distribution, and zeta potential. D-mannitol was added as a cryoprotectant to the undiluted nanoparticles before being lyophilized with an Alpha 2-4 LD plus CHRIST lyophilizer (Germany) to prevent particle aggregation (Fukushima *et al.,* 2007).

CHARACTERIZATIONS OF SLY-DH-CNPS

A. Transmission Electron Microscopy Analysis

Transmission electron microscopy was used to examine the size and morphological characteristics of SLY-DH-CNPs (TEM). Using a formvar carbon-coated 200 mesh copper TEM grid, a few drops of diluted SLY-DH-CNPs solutions were applied. The grid was then negatively stained for 10 minutes with 1% uranyl acetate and lead acetate (w/v) before being let to dry. The instrument was adjusted after inserting the grid into the specimen holder. Transmission electron microscopy (TEM) pictures of NPs were captured using a JEOL-JSM-1400 PLUS (Peabody, MA, USA) (Robinson *et al.,* 1988).

B. SEM (Scanning Electron Microscopy) Analysis

The created SDNPs nanoformulation's shape and structure were investigated using a SEM, the Nova Nano SEM 450, from Germany. Prior to the SEM analysis, the formulations were lyophilized using a freeze-dry lyophilizer (REMI, New Delhi, India). The dried formulations were then attached to a SEM stub using dual adhesive tape utilising a sputter (KYKY SBC-12, Beijing, China) at 50 mA for 5 to 10 minutes (Hafez *et al.,* 2017). The developed SLY-DH-CNPs nanoformulation was photographed using a SEM equipped with a secondary electron detector.

C. Dynamic Light Scattering and Zeta Potential Analysis

Particle size (hydrodynamic diameter) and polydispersity index (PDI) were determined using dynamic light scattering (DLS), and ZP measurements of SLY-DH-CNPs were carried out three times for each sample at 25°C on a Zetasizer Nano ZS (Nano and zeta Sizer Malvern, Grove, UK) with a backscattering detection angle of 173°. The nanoparticle samples were sonicated and diluted with ultrapure distilled water before analysis (Liu *et al.,* 2018).

D. Drug Entrapment Efficiency and Loading Capacity

Entrapment efficiency is the proportion of pharmaceuticals that are trapped inside the nanoparticles to all medications (EE). In a nutshell, 10 mL of SLY-DH-CNP suspension were spun at 15,000 rpm for 30 minutes at 4 °C to separate it from the SLY-DH-containing aqueous medium. The sample was then re-mixed with ultra-pure water. A UV spectrophotometer was used to measure the

concentration of SLY-DH in the supernatant at 287 nm after it had been diluted. Standard SLY-DH concentrations were plotted against absorbance to create a calibration curve (Bansal and Chamroonkul 2019). The following equations were used to determine the drug loading capacity (LC%) and effective exposure (EE%) of SIL in SLY-DH-CNPs (Ebrahimi *et al.,* 2018).

EE % = (Amount of SIL added − free SIL in supernatant)/ Amount of SIL added × 100

LC % = (Amount of SIL added − free SIL in supernatant)/ Nanoparticles weight × 100

E. In Vitro Drug Release Study

The in vitro release of SLY-DH-CNPs was examined for 48 hours at various pH levels of 5 and & for both qualitative analysis and concurrent toxicity analysis. After inserting the dosage form of SLY-DH-CNPs into the release media, which is maintained at a constant temperature, the release of the pharmaceuticals is assessed by sampling and SLY-DH detection in the release media. In a nutshell, 10 mg of the dry powdered produced SLY-DH-CNPs sample was dissolved in 10 mL of PBS containing 0.1% tween 20 (Gillessen and Schmidt 2020). It was then incubated at 37°C and 250 rpm in a shaking water bath. To keep the total volume constant until the end of the experiment and analyse the release kinetics of the SLY-DH, 5 mL of supernatant was removed at the time intervals 1, 2, 4, 8, 12, 16, 18, 20, 22 and 24 and replaced with 5 mL of fresh dissolving medium at 37 0.5°C. By measuring the absorbance of solutions at 287 nm, the medication released in these fractions was assessed. By translating the drug concentration into a percentage of the total drugrelease using the formula below, the drug release statistics were adjusted (De Avelar *et al.,* 2017).

% of cumulative drug release = Released SIL from NPs at time/ Amount of SIL added in NPs × 100

F. In Vivo Study

(a) Animals. Thirty male Wistar albino rats that were clear of pathogens and weighed about 250 10 g when they were 3–4 months old were used. The animals came from the public veterinary institution in Mhou, MP, India. The animals were kept in individually ventilated cages at a constant temperature of 22 °C with a 12:12 hour light/dark cycle. They had unlimited access to food and water, as well as consistent environmental conditions both before and after the experiment. Before the tests began, all animals spent two weeks becoming acclimated in the lab (Lim and Kim 2008).

(ii) Ethical Statement. The study follows ARRIVE protocols and complies with the National Research Council's guide for the care and use of laboratory animals (Geervliet and Bansal 2020). All operations were carried out in compliance with the institutional animal ethical committee's recommendations no. PCP/IAEC/2023/JAN/10

(iii) Establishment of Liver Fibrosis Model. To cause liver fibrosis, rats were given intraperitoneal (i.p.) injections of carbon tetrachloride (CCl4) (1 mL/kg) dissolved in olive oil (1:1 v/v) three times per week for ten weeks, and subsequently once per week for two weeks (Abenavoli *et al.,* 2011).

The animals were divided into five groups, each with six rats: the normal control group (G1), the rats received an intraperitoneal injection of normal saline, the toxic control group (G2), or the negative control group, in which fibrosis was produced using CCl4 and no treatment was given. Group 3 (G3) refers to the typical control group that delivered fibrosis coupled with a standard medication solution of L-Ornithine and L-Aspartate (Nagpal *et al.,* 2013). The treatment group was depicted in group 4 (G4) at a dose of 25 mg/kg SLY-DH-CNPs and 100 mg/kg in olive oil. The treatment group displayed SLY-DH-CNPs with fibrosis and group 5 (G5) at a dose of 50 mg/kg SLY-DH-CNPs with a dose of 100 mg/kg in olive oil. During 30 days, all therapies were given via oral gavage (Maksoud *et al.,* 2019).

(iv) Sample Collection and Tissue Preparation. All of the animals were overnight starved, weighed, and given a deep isoflurane inhalation to put them to sleep at the conclusion of the treatment period. After being drawn from the heart, the blood samples were centrifuged at 3000 rpm for 20 minutes at 4 C to separate the sera for the biochemical analysis. In order to determine the liver index, the livers were separated, cleaned, and weighed (Draper and Hadley1990).

Liver Index Calculation = [Liver weight (g)/Body weight (g)] × 100

Three aliquots of the liver tissues were prepared: one was processed in 10% normal formalin for H&E staining, Masson's trichrome staining (MT), and immunohistochemistry (IHC). To prepare the remaining sample for ELISA and lipid peroxidation assays, it was homogenised in cold, 0.1 mM PBS in a ratio of 1:9 (Livak and Schmittgen 2001).

(v) Methods. Blood Biomarkers for Testing Liver Function Total bilirubin and albumin levels, as well as the activities of the enzymes aspartate aminotransferase (AST), alanine aminotransferase (ALT), and alkaline phosphatase (ALP), were assessed using commercially available kits (Biosystems S.A. Costa Brava 30, Barcelona, Spain) in accordance with the manufacturer's guidelines(Suvarna *et al*., 2019).

(vi) Malondialdehyde (MDA) as Index of Lipid Peroxidation. Using the Draper and Hadley method, MDA in homogenate was measured for thiobarbituric acid reactive compounds (TBARS). Thiobarbituric acid (TBA) was used to heat the sample at a low pH. (3.5). At 532 nm, the absorbance of the resultant pink chromogen was measured (Wu *et al*., 2019).

(vii) Histopathology Study. The liver tissues were collected rapidly, subjected to a 24-hour treatment in 10% neutral-buffered formalin, dehydrated in ethanol at increasingly higher concentrations (from 70% to 100%), cleaned in xylene, and then embedded in paraffin. Slices of paraffin, five micron thick, were cut with a microtome (Leica RM 2155, London, UK). Hematoxylin and eosin (H&E) was used to stain the sections for histopathology [106]. Leica® microscopes (Wetzlar, Germany) and an Am Scope® microscope digital camera were used to obtain all section

photographs. On sections stained with MT stain, ImageJ software was used to conduct a quantitative analysis of liver fibrosis (as a percentage) (Image J 1.47v, National Institute of Health, Bethesda, MD, USA)(Li *et al.,* 2003). The blue-stained area measurements in the samples, which were made for images with at least 10 different fields per section at a magnification level of about 100, were always synchronised with the colour settings in the ImageJ software. Scores for each fibrosis stage were determined using the following criteria: Score 0 indicates no fibrosis; 1 indicates a little fibrosis; 2 indicates mild fibrosis; 3 indicates considerable fibrosis; and 4 indicates severe fibrosis. The evaluation was already explained (Hsu *et al.,* 1981).

G. Statistical Analysis

Mean ± SD was used to express the values. Statistics. One-way analysis of variance (ANOVA) was used to statistically analyse the data, and a result of $p>0.01$ ($n = 3$) was deemed significant (Gabius and Gabius 2012).

RESULTS AND DISCUSSION

A. Synthesis of SLY-DH-CNPs

The chitosan nanoparticles encasing the SM-DH were spontaneously synthesised after the pawn anion TPP was added to the steady Chitosan polymer solutions. Nanoparticles were created as a result of ionic interactions between the positively charged amino groups of chitosan and the negatively charged ion TPP. The CS/TPP ratio was adjusted to produce steady dispersion and nanosize particles. Preliminary tests were done to establish the best CS and TPP concentrations for the synthesis of NPs. Both the method and formulation parameters were fine-tuned to create physiochemically and thermally stable nanoparticles. The three primary forms of the acquired particles were a transparent solution, an opalescent suspension with a tyndall effect (NPs), or other kinds of extensively documented nano-sized particles.

B. TEM Analysis of SLY-DH-CNPs

The SLY-DH-CNPs' size and shape were verified using TEM evaluations. The TEM images of SCNPs in Fig. 1 a demonstrate that they are distributed as independent NPs with a distinct spherical shape and are uniformly spread, with an average particle size of 140 ± 2 nm.

C. SEM Analysis

SEM examination significantly enhanced the Zeta sizer and TEM assay results that showed the production of tiny particles with a smooth morphology and spherical form. The SEM images particularly highlight and validate the nanoformulation's crisp oval borders, which demonstrated a better synthesis procedure. Also, it is evident from the SEM images that there is no sign of particle aggregation or cluster formation with an apparent PEG outer layer. The zeta-sizer study and the SEM examination, both of which indicated size ranges of 120-190 nm, verified the outstanding brain targeted delivery properties of SLY-DH-CNPs (Fig. 1b).

D. DLS and Zeta Potential Measurements of SLY-DH-CNPs

The particle size distribution curves for SLY-DH-CNPs showed only one peak and a low polydispersity index. SLY-DH-CNPs were found to have a particle size of 170.4 nm. The findings revealed that the SLY-DH-CNP sample under investigation had extremely positively charged values at +26.3 mV, indicating that the synthesized NPs had higher dynamic stability as shown in Fig. 1c-e.

E. Drug Entrapment Efficiency and Loading Capacity of SLY-DH-CNPs

For the examination of nanoparticle qualities, entrapment efficiency (EE%) and drug loading capacity (LC%) are thought to be important metrics. Silymarin (SLY) and Dehydroemetine (DH) content in supernatant was used to determine the EE% of SLY-DH-CNPs. The results showed that more than 90.16 ±1.67% of the drug combination was trapped in polymer content. LC% value, on the other hand, was 18.26 ± 2.15%.

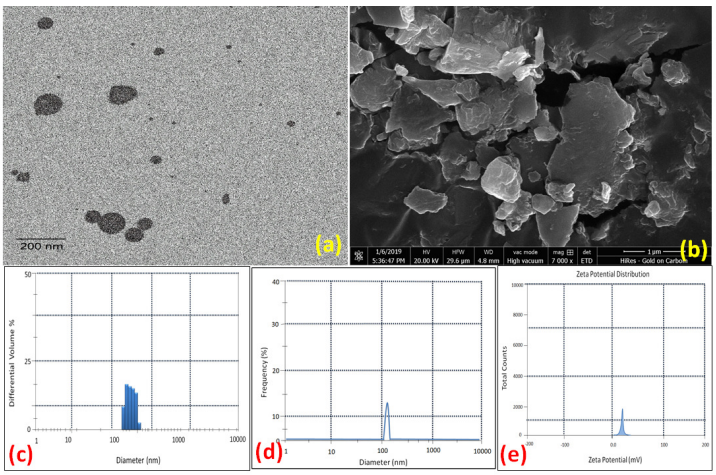

Fig. 1. Image a & b illustrating TEM and SEM investigation of developed SYL-DH-CNPs at nano scale resolution respectively, whereas image c elaborating size distribution pattern by zeta sizer measurement, image d & e showing the DLS pattern and zeta potential of developed SYL-DH-CNPs respectively, (mean ± SD, n=3).

F. In Vitro Drug Release Study

According to the data gathered from the release studies, the release profile of developed SLY-DH-CNPs was investigated in vitro using PBS (pH 5 & 7.4) at 37 0.5 C. The cumulative amount of drug combination of SLY-DH released percentage (%) at specific different time intervals was plotted versus time (h). A typical two-phase release pattern was demonstrated in vitro, as shown in Fig. 2 a-b. The first phase of the release pattern showed a burst and release that happened relatively quickly at a specific time (about 50% of the entrapped SLY-DH released in 4 h), followed by a sustained and gradual release phase that happened over a long period of time at pH 5 and showed acidic release of chitosan nanoparticles. While 30% of the drug was released from SLY-DH-CNPs over the first 24 hours at pH 7, revealing a meagre release pattern at normal pH, approximately 86% of the drug was released around 24 hours at pH 5. The initial quick release that was seen may have been caused by the drug dispersing on the surface of the SLY-DH-CNPs, which was followed by a slower, longer release of the SLY-DH-CNPs.

G. In Vivo Studies

(i) Body Weight Gain, Liver Weight, and Liver Index (%). CCl4 exposure raised liver weight and liver index while dramatically reducing body weight gain as compared to the control group (Fig. 2 c-e). The best result was observed in rats treated with SCNPs, which displayed entirely normal values. CCL4-intoxicated rats treated with any of the treatments acquired noticeably more body weight and had lower liver weight and liver index values than the CCl4-untreated group.

Fig. 2. Image a and b elaborating the combination drug release kinetics of developed SYL-DH-CNPs at pH 5 and 7 using dialysis bag membrane, whereas images c-e showing effect of different groups on body weight gain, liver weight, and liver index (%). Data are presented as mean ± SD (n = 6) according to the ANOVA test, followed by the student T test. At $p \leq 0.05$, the difference was statistically significant.

(ii) Serum Liver Function Markers. When compared to control rats, CCl4-rats exhibit noticeably higher AST, ALT, and ALP serum activity as well as bilirubin levels and noticeably lower albumin levels. When compared to untreated rats, CCl4-rats treated with SIL, CNPs, or SCNPs exhibit significant improvements in all liver serum markers. The SCNPs-treated CCl4-rats displayed the best effects, with no discernible changes from the control rats (Fig. 3 a-e).

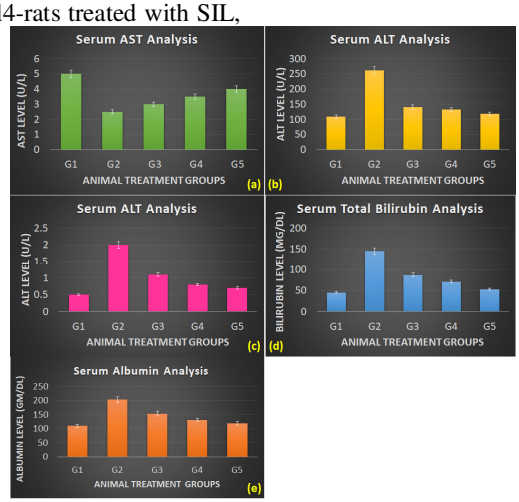

Fig. 3. Images a-e elaborating effects of developed SYL-DH-CNPs on serum liver function parameters. Data are presented as mean ± SD (n = 6) according to the ANOVA test, followed by the student T test. At $p \leq 0.05$, the difference was statistically significant.

(iii) Histopathology. Images of a gross examination of the liver following animal excision are shown in Fig. 4 a-e. The livers in the olive oil-treated control group were healthy and had a soft, smooth, and shiny exterior. However, the liver of CCl4-intoxicated rats had a nodular appearance, a rough, stiff, hard spotty surface, and no lustre; in addition, the faint red colour showed the flow of blood through the liver had diminished, reflecting fibrosis in human livers. The rats given CNPs showed modest liver morphological abnormalities after treatment. Compared to CCL4-untreated rats, the livers of SIL-treated rats had smoother surfaces and less nodular abnormalities. Rat livers with dramatically enhanced physical appearance, a much healthier look, and bright, shiny, and smooth surfaces as a result of SYL-DH-CNPs therapy effectively reduced CCl4-induced hepatic fibrosis.

(iv) Histopathology of Liver Tissue. All hepatic architectures, the central vein and hepatic cords, hepatocytes, sinusoids, and the portal triad were all normal in the livers of control rats. The hepatic vein was noticeably enlarged, the blood vessels were clogged, and there was obvious portal fibrosis with the deposition of mature collagen fibrils and fibroblast hyperplasia in the CCl4-rat liver sections. The ameliorative effects of the previous alteration were present in variable degrees in the treated groups. The liver sections of the rats treated with CNPs showed localised necrosis, which was replaced by necrotic debris and extravasated erythrocytes, whereas the SYL-DH-treated rats displayed mild to moderately pyknotic hepatocytes congested and enlarging sinusoids. Rats that received SYL-DH-CNPs had liver sections that appeared to have typical hepatic architecture, including diplocytes on the few hepatocytes and a small enlargement of the sinusoids (Fig. 4 a-e).

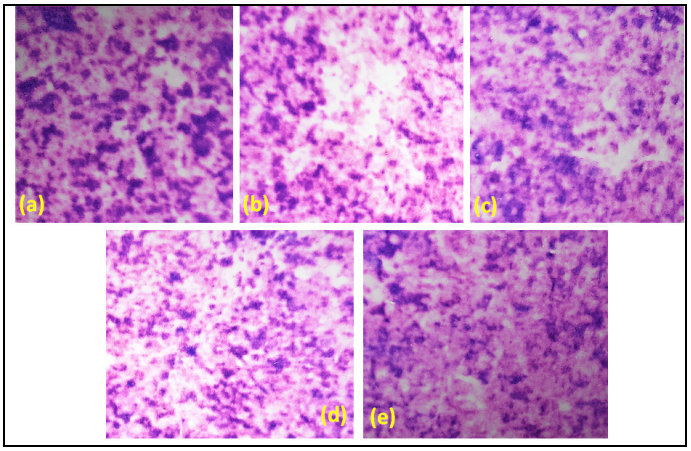

Fig. 4. Images (a-e) showing histopathology slides of different treatment groups (G1: a, G2: b, G3:c, G4: d, G5: e) of liver cells visualized at 100X lens magnification using light microscope (Olympus, Japan), $p<0.01$, $n=3$.

CONCLUSIONS

In the current study, we used the ionotropic gelation process to successfully create Silymarin-Dehydroemetine-loaded chitosan nanoparticles (SYL-DH-CNPs). The created nanoparticles have physicochemical characteristics that were optimal for effectively delivering Silymarin-DH to target liver cells. When compared to free drug combination the SYL-DH-CNPs in vitro drug release demonstrated greater drug release and bioavailability. Also, the in vivo study's findings showed that, when compared to drug itself, the generated SYL-DH-CNPs shown better effects against CCl4 toxicity-induced liver fibrosis with lower oxidative damage and improved antioxidant defence system. This could happen via down regulating the main fibrosis mediators by targeting and enhancing the hepatic expression. Together with the enhanced bio pharmacokinetics lowering level and the decrease of oxidative stress, these results led to the inhibition of the pathogenic pathways responsible for the formation of liver fibrosis, chronic inflammation, and collagen deposition. These findings imply that the oral distribution of SYL-DH in its nanoformulation with SYL-DH-CNPs is a feasible alternative for its potential therapeutic use in the treatment of liver fibrosis. Additionally the usage and delivery of biodegradable chitosan based SLY-DH nanoparticles may increase the bioavailability at the desired site bypassing the systemic toxicity and decreasing the dose duration with dose regimen. In building the targeted drug delivery system against the liver ailment not only decrease the heavy dose dependency of conventional dosage form but also provide the novel therapeutics system against liver disease with negligible toxicity and cost economic management.

Acknowledgement. I extend my sincere thanks to Professor Neeraj Sharma & Professor Ritesh Jain and to my advisory committee member for giving me proper guidance throughout the course of study.

Conflict of Interest. None.

REFERENCES

Abenavoli, L., Aviello, G., Capasso, R., Milic, N. and Capasso, F. (2011). Milk thistle for treatment of nonalcoholic fatty liver disease. *Hepat. Mon. 11*, 173–177.

Arfmann-Knübel, S., Struck, B., Genrich, G., Helm, O., Sipos, B., Sebens, S., and Schäfer, H. (2015). The crosstalk between Nrf2 and TGF-β1 in the epithelial-

mesenchymal transition of pancreatic duct epithelial cells. *PLoS ONE , 10*, e0132978.

Bansal, M. B. and Chamroonkul, N. (2019). Antifibrotics in liver disease: Are we getting closer to clinical use? *Hepatol. Int., 13,* 25–39.

Choi, H. K., Pokharel, Y. R., Lim, S. C., Han, H. K., Ryu, C. S., Kim, S. K., Kwak, M. K. and Kang, K. W. (2009). Inhibition of liver fibrosis by solubilized coenzyme Q10: Role of Nrf2 activation in inhibiting transforming growth factor-β1 expression. *Toxicol. Appl. Pharmacol., 240*, 377–384.

De Avelar, C. R., Pereira, E. M., De Farias Costa, P. R., De Jesus, R. P. and De Oliveira, L. P. (2017). Effect of silymarin on biochemical indicators in patients with liver disease: Systematic review with meta-analysis. *World J. Gastroenterol., 23*, 5004.

Draper, H. and Hadley, M. (1990) Malondialdehyde determination as index of lipid Peroxidation. *Methods Enzymol., 186,* 421–431.

Ebrahimi, H., Naderian, M. and Sohrabpour, A. A. (2018). New concepts on reversibility and targeting of liver fibrosis; A review article. *Middle East J. Dig. Dis., 10*, 133.

Fukushima, T., Hamada, Y., Yamada, H. and Horii, I. (2007). Changes of micro-RNA expression in rat liver treated by acetaminophen or carbon tetrachloride− regulating role of micro-RNA for RNA expression. *J. Toxicol. Sci., 32,* 401–409.

Gabius, H. J. and Gabius, S. (2012). Lectins and Glycobiology; Springer Science & Business Media: Berlin/Heidelberg, Germany.

Geervliet, E. and Bansal, R. (2020). Matrix metalloproteinases as potential biomarkers and therapeutic targets in liver diseases. *Cells, 9*, 1212.

Gjorgjieva, M., Sobolewski, C., Ay, A. S., Abegg, D., Correia de Sousa, M., Portius, D., Berthou, F., Fournier, M., Maeder, C. and Rantakari, P. (2020). Genetic ablation of MiR-22 fosters diet-induced obesity and NAFLD development. *J. Pers. Med., 10*, 170.

Gillessen, A. and Schmidt, H. H. J. (2020). Silymarin as supportive treatment in liver diseases: A narrative review. Adv. *Ther., 37,* 1279–1301.

Hafez, M. M., Hamed, S. S., El-Khadragy, M. F., Hassan, Z. K., Al Rejaie, S. S., Sayed-Ahmed, M. M., Al-Harbi, N. O., Al-Hosaini, K. A., Al-Harbi, M. M. and Alhoshani, A. R. (2017). Effect of ginseng extract on the TGF-β1 signaling pathway in CCl4 -induced liver fibrosis in rats. BMC Complement. *Altern. Med., 17,* 45.

Hsu, S. M., Raine, L. and Fanger, H. (1981). A comparative study of the peroxidase-antiperoxidase method and an avidin-biotin complex method for studying polypeptide hormones with radioimmunoassay antibodies. *Am. J. Clin. Pathol., 75*, 734–738.

Hobert, O. (2008). Gene regulation by transcription factors and microRNAs. *Science, 319*, 1785–1786.

Hong, Y., Cao, H., Wang, Q., Ye, J., Sui, L., Feng, J., ... & Chen, X. (2016). MiR-22 may suppress fibrogenesis by targeting TGFβR I in cardiac fibroblasts. *Cellular physiology and biochemistry*, *40*(6), 1345-1353.

Ji, D., Li, B., Shao, Q., Li, F., Li, Z. and Chen, G. (2015). Mir-22 suppresses bmp7 in the development of cirrhosis. Cell. *Physiol. Biochem., 36*, 1026–1036.

Jiao, J., Friedman, S. L. and Aloman, C. (2009). Hepatic fibrosis. *Curr. Opin. Gastroenterol., 25*, 223.

Jiang, X. P., Ai, W. B., Wan, L. Y., Zhang, Y. Q. and Wu, J. F. (2017). The roles of microRNA families in hepatic fibrosis. *Cell Biosci., 7*, 34.

Liu, L., Wang, Q., Wang, Q., Zhao, X., Zhao, P., Geng, T. and Gong, D. (2018). Role of miR29c in goose fatty liver is mediated by its target genes that are involved in energy homeostasis and cell growth. *BMC Vet. Res., 14*, 325.

Laouar, A., Klibet, F., Bourogaa, E., Benamara, A., Boumendjel, A., Chefrour, A. and Messarah, M. (2017). Potential antioxidant properties and hepatoprotective effects of *Juniperus phoenicea* berries against CCl_4 induced hepatic damage in rats. *Asian Pac. J. Trop. Med., 10*, 263–269.

Lim, Y. S. and Kim, W. R. (2008). The global impact of hepatic fibrosis and end-stage liver disease. *Clin. Liver Dis. 12*, 733–746.

Livak, K. J. and Schmittgen, T. D. (2001). Analysis of relative gene expression data using real-time quantitative PCR and the 2(-Delta Delta C(T)) Method. *Methods, 25*, 402–408.

Li, C., Luo, J., Li, L., Cheng, M., Huang, N., Liu, J. and Waalkes, M. P. (2003). The collagenolytic effects of the traditional Chinese medicine preparation, Han-Dan-Gan-Le, contribute to reversal of chemical-induced liver fibrosis in rats. *Life Sci. 72*, 1563–1571.

Maksoud, H. A., Magid, A. D. A., Mostafa, Y., Elharrif, M. G., Sorour, R. I. and Sorour, M. I. (2019). Ameliorative effect of liquorice extract versus silymarin in experimentally induced chronic hepatitis: A biochemical and genetical study. *Clin. Nutr. Exp., 23*, 69–79.

Mohseni, R., Karimi, J., Tavilani, H., Khodadadi, I. and Hashemnia, M. (2019). Carvacrol ameliorates the progression of liver fibrosis through targeting of Hippo and TGF-β signaling pathways in carbon tetrachloride (CCl_4)-induced liver fibrosis in rats. *Immunopharmacol. Immunotoxicol, 41*, 163–171.

Nagpal, K., Singh, S. K. and Mishra, D. N. (2013). Optimization of brain targeted gallic acid nanoparticles for improved antianxiety-like activity. *Int. J. Biol. Macromol., 57*, 83–91.

Noyan, S., Çavu¸so ˘glu, ˙I. and Minbay, F. Z. (2006). The effect of vitamin A on CCl4 -induced hepatic injuries in rats: A histochemical, immunohistochemical and ultrastructural study. *Acta Histochem, 107*, 421–434.

O'Reilly, S. (2016). MicroRNAs in fibrosis: Opportunities and challenges. *Arthritis Res. Ther., 18*, 11.

Reddy, A. S., Lakshmi, B. A., Kim, S. and Kim, J. (2019). Synthesis and characterization of acetyl curcumin-loaded core/shell liposome nanoparticles via an electrospray process for drug delivery, and theranostic applications. *Eur. J. Pharm. Biopharm, 142,* 518–530.

Robinson, T. F., Cohen-Gould, L., Factor, S. M., Eghbali, M. and Blumenfeld, O. O. (1988). Structure and function of connective tissue in cardiac muscle: Collagen types I and III in endomysial struts and pericellular fibers. *Scanning Microsc., 2*, 1005–1015.

Roulot, D., Sevcsik, A. M., Coste, T., Strosberg, A. D. and Marullo, S. (1999). Role of transforming growth factor β type II receptor in hepatic fibrosis: Studies of human chronic hepatitis C and experimental fibrosis in rats. *Hepatology., 29*, 1730–1738.

Suvarna, K. S., Layton, C. and Bancroft, J. D. (2019). Bancroft's Theory and Practice of Histological Techniques E-Book; Elsevier Health Sciences: Amsterdam, *The Netherlands, 4*, 441-449.

Sethi, L, Suri, S., Sarma, K. and Sasan, J. S. (2021). Histomorphology and Histochemistry of Liver of Adult Bakerwali and Non-descript Goats of Jammu, India. *Journal of Animal Research, I*(3), 487-495.

Supriono, S., Nugraheni, A., Kalim, H., & Eko, M. H. (2019). The effect of curcumin on regression of liver fibrosis through decreased expression of transforming growth factor-β1 (TGF-β1). *The Indonesian Biomedical Journal*, *11*(1), 52-8.

Thakur, P. N. and Kapadnis, P. J. (2021). Gross observations of liver in buftälo (*Bubalus bubalis*). *Buffalo Bulletin, 40*(1), 1-5.

Wu, Y. C., Huang, H. H., Wu, Y. J., Manousakas, I., Yang, C. C. and Kuo, S. M. (2019). Therapeutic and Protective Effects of Liposomal Encapsulation of Astaxanthin in Mice with Alcoholic Liver Fibrosis. *Int. J. Mol. Sci., 20*, 4057.

Zhang, Y., Liu, J., Ma, Y., Wang, J., Zhu, J., Liu, J. and Zhang, J. (2019). Integration of high-throughput data of microRNA and mRNA expression profiles reveals novel insights into the mechanism of liver fibrosis. *Mol. Med. Rep., 19*, 115–124.

How to cite this article: Saurabh Arjariya, Ritesh Jain and Neeraj Sharma (2023). Development and Characterization of Chitosan-Functionalized Biodegradable Nanoparticles for the Enhanced Hepatoprotective Effects Against Liver Fibrosis. *Biological Forum – An International Journal, 15*(3): 161-168.